

**United States
Department of
Agriculture**

**Natural
Resources
Conservation
Service**

**c/o USDA Forest Service
11 Campus Boulevard
Suite 200
Newtown Square, PA 19073
(610) 557-4233; FAX: (610) 557-4200**

Subject: SOI – Ground-penetrating radar (GPR) study of ice-wedge networks
at Barrow, Alaska

Date: 9 August 2011

To: Dr. Fredrick E. Nelson
Department of Geography
University of Delaware
207 Pearson Hall
Newark, DE 19716

Dr. Ken Hinkel
Department of Geography
University of Cincinnati
400F Braunstein
Cincinnati, OH 45221-0131

Participants:

Jim Doolittle, Research Soil Scientist, USDA-NRCS-NSSC, Newtown Square, PA
John Kimble, Retired Research Soil Scientist, Addison, NY
Ken Hinkel, Professor, Geography Department, University of Cincinnati, Cincinnati, OH
Fritz Nelson, Professor, Geography Department, University of Delaware, Newark, DE

Activities:

All field activities were completed on 2 to 5 April 2011.

Summary:

Two-dimensional (2D) ground-penetrating radar (GPR) records were used to construct a three-dimensional (3D) pseudo-image of ice-wedge polygons across a 0.25 hectare area near Barrow, Alaska. These graphic displays greatly improved the quality of radar interpretations of ice wedges and ice-wedge polygons. Time-slices of a 3D pseudo-image were used to illustrate the geometry and trends of ice-wedge networks. Compared with 2D radar interpretations of ice wedges and ice-wedge polygons, 3D data interpretations are more complete and less ambiguous.

On 2D radar records, distinct hyperbolic patterns were associated with ice-wedges. Ice wedges are characterized by a shallow set of relatively shallow hyperbolas, and an underlying secondary set of hyperbolas. These multiple hyperbolic reflections provide a distinguishing *hyperbolic facies*, which can aid the identification of ice wedges. The lower set of hyperbolas has been associated with the bottom of the ice wedges and the contact with the underlying soil materials (Bertram et al., 1972). Others have attributed the secondary hyperbolas to refractions of the propagated waveform inside the ice wedge and oblique reflections from the vertically foliated ice and the ice-wedge wall. More work needs to be done to identify the source(s) of these secondary hyperbolas.

A radar traverse was conducted across the margins of a thaw lake. Major reflectors identified on 2D radar records included the snow/ice interface, ice/soil interface, and ice-bottom multiples. Several distinct zones of signal weakening were identified and associated with scattering losses from segregated ice crystals and the presence of greater amounts of free water. A reflector believed to represent the permafrost table was identified on the radar

record. This linear reflector appears wavy beneath the deeper portions of the thaw lake, but becomes more parallel with the ice/soil interface as the ice thins and the lake shallows.

The location of an all-terrain vehicle trail is difficult to discern by subsurface GPR imagery alone. While the ability of GPR to detect differences in the subsurface is not doubted, additional field work is necessary to improve pattern recognition associated with trails on radar records.

With kind regards,

James A. Doolittle
Research Soil Scientist
National Soil Survey Center
c/o USDA Forest Service
11 Campus Blvd., Suite 200
Newtown Square, PA 19073

Background:

Soils underlain by permafrost (Gelisols) are profoundly influenced by cryoturbation and ice segregation (Soil Survey Staff, 1999). These processes are manifested by sharp discontinuities, small-scale heterogeneities, and complex morphologies in gelic materials. Cryoturbation results in irregular and broken horizons, involutions and accumulations of contrasting soil materials. The segregation of ice is manifested in different forms of ice masses (e.g. ice lenses, vein ice, segregated ice crystals, and ice wedges (Soil Survey Staff, 1999)). The formation of ice wedges and ice-wedge polygons is attributed to the segregation of ice.

Ice wedges and ice-wedge polygons are features found only in permafrost regions. Ice wedges are wedge-shaped, foliated ground ice that form in perennial frozen ground as a result of thermal contraction (American Geologic Institute, 1980). Ice wedges can occur as vertical or inclined sheets, dikes, or veins that taper downward and measure from a few millimeters to as much as 6 meters wide at the surface, and from 1 to as much as 30 meters deep (American Geologic Institute, 1980). Extremely cold soil temperatures and thermal contraction are factors responsible for the development of ice wedges. Ice wedges result from the repeated, annual filling of thermal contraction cracks with hoar-frost or snow melt waters (Brown, 1967). During warmer months, permafrost expands causing horizontal compression and the displacement of the bordering soil materials (Price, 1972). In the colder months, renewed thermal contraction occurs in the zone of weakness formed by the ice wedge (Price, 1972). Through this repeated cycle, ice wedges grow, adjoining soil materials are compacted and displaced, furrows develop over ice wedges, and extensive honeycomb systems of ice-wedge polygons are formed. Ice wedges are often expressed on the soil surface as distinct surface linear furrows (Figure 1). Though easily located in most instances, Arcone et al. (1982) noted that some deeply buried wedges, shallow inactive wedges, and smaller wedges may not have surface manifestations.



Figure 1. Ice-wedge polygons, a form of patterned ground, are conspicuous landforms in the Barrow area (photograph courtesy of Ben Jones).

A network of intersecting ice-wedges forms an ice wedge polygons (see Figures 1 and 2). In the Barrow area, it is estimated that about 65 % of the land surface is covered by ice-wedge polygons (Brown, 1967). As evident in Figure 1 and 2, ice-wedge polygons are 3- to 6-sided features with interconnected, straight to gently curving furrows that are formed by ice wedges. The furrows overlie ice-wedges, vary in width, and can be several hundreds of meters long (Mangold et al., 2005). The furrows typically have orthogonal junctions. Ice-wedge polygons are

classified based on the relative elevation of the polygon's center with respect to its margins. *Low-center polygons* have margins that are upturned to form low ridges, while *high-center polygons* have downturned margins. The diameter of individual ice-wedge polygons varies from a few to as much as 150 m and is dependent upon the age and spacing of ice wedges (Price, 1972). Relief of ice-wedge polygons is generally about 15 to 45 cm (Hussey and Michelson, 1966).

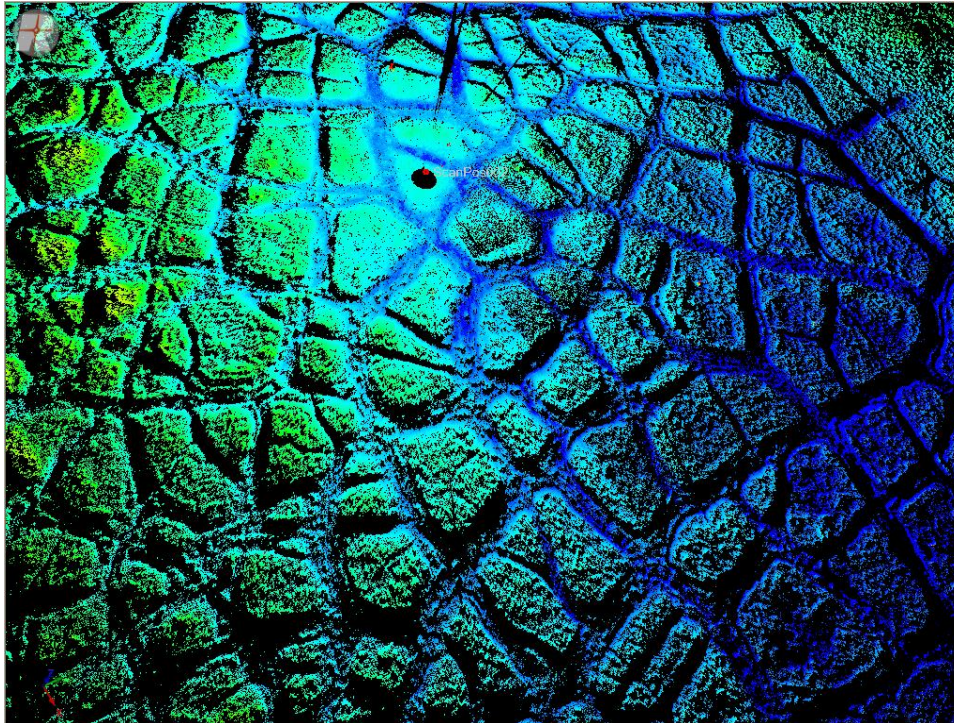


Figure 2. A network of intersecting ice-wedge forms ice-wedge polygons near "CRREL site" of the Barrow Environmental Observatory. This image is from a ground-based Lidar survey made in August 2010 by Marianne Okal of UNAVCO, under the auspices of the CALM program.

The principal objective of this field research was to use ground-penetrating radar (GPR) to investigate the subsurface structure and configuration of ice-wedge polygons near Barrow, Alaska. Previous work by the participants is described in Munroe et al. (2007).

Ground-Penetrating Radar:

Ground-penetrating radar (GPR) is a non-invasive, high-resolution geophysical method used in near-surface explorations. Ground-penetrating radars transmit short pulses of high to ultra high frequency (center frequencies from 12.5 MHz to 2.6 GHz) electromagnetic energy into the ground to detect subsurface interfaces. A time-scaled system, GPR measures the time that it takes pulses of electromagnetic energy to travel from an antenna to a subsurface interface and back. Interfaces often correspond to major soil, stratigraphic, and lithologic layers or features. Whenever a pulse contacts an interface separating layers with different relative dielectric permittivity (E_r), a portion of the energy is reflected back to a receiving antenna. The more abrupt and contrasting the permittivity on opposing sides of an interface, the greater the amount of energy that is reflected back to the antenna and the greater the amplitude of the recorded signal. To convert the pulse travel time into a depth scale, the velocity of pulse propagation or the depth to a reflector must be known.

A useful feature of GPR is its ability to rapidly acquire high-resolution images of the subsurface, which aid the lateral extension of information obtained at coring sites, and the vertical extension of observations made of features exposed at the soil surface. Since the 1970s, GPR has been used extensively in areas of permafrost. In general, permafrost provides physical properties that are more conducive to GPR than encountered in similar non-frozen materials. As the temperature falls below 0° C, the electrical conductivity, dielectric permittivity, and loss tangent

of earthen materials decrease, while the velocity of radar pulse propagation increases (Scott et al., 1990). As water freezes in soils, energy losses attributable to electrical conductivity and molecular polarization decrease, and the penetration depth of GPR is increased. Owing to the strong contrast in dielectric permittivity between unfrozen and frozen materials, GPR has been used extensively in permafrost to detect materials containing varying amounts of liquid and frozen water. Hinkel et al. (2001) demonstrated that the contrast in dielectric properties between an ice wedge and surrounding frozen soil matrix is sufficient to produce identifiable, high-amplitude reflections on radar records.

Ground-penetrating radar has been used to measure the relative dielectric permittivity of frozen sediments (Annan et al., 1975; Annan and Davis, 1976; Davis et al., 1976; Arcone and Delaney 1982, 1984, 1989; Arcone et al., 1998). In addition, GPR has been used to study spatial and temporal variations in the thickness of the active layer and the depths to the permafrost table (Wong et al., 1977; Annan and Davis 1978; Pilon et al., 1979, 1985; Doolittle et al., 1990, 1992; Moorman et al., 2003; Wu et al., 2005). It has also been used to identify and map areas of massive ground ice and ice wedges (Bertram et al., 1972; Kovacs and Morey, 1979, 1985; Arcone et al., 1982; Dallimore and Davis, 1987; Scott et al., 1990; Robinson et al., 1993; Hinkel et al., 2001; De Pascale et al., 2008), buried glacier ice (Brandt et al., 2007), taliks (Arcone et al., 1998) and ice-wedge and sediment-filled wedge polygons (Hinkel et al., 2001; Fortier and Allard, 2004; Munroe et al., 2007; Doolittle and Nelson, 2008 and 2009; Godfrey et al., 2008; and Watanabe et al., 2008). It has also been used to identify the internal structure and composition of pingos (Kovacs and Morey, 1985; Ross et al., 2005; Yoshikawa et al., 2006), palsas (Sequin, 1986; Doolittle et al., 1992; Horvath, 1998), and rock glaciers (Leopold et al., 2011). Although applications have been more limited, because of accessibility and terrain conditions, GPR has found to be ill-suited to mapping mountain permafrost (Vonder Mühll et al., 2002).

While the physical properties of permafrost are favorable to deeper GPR profiling, cryoturbated soil horizons are difficult to resolve and therefore distinguish on radar records. Cryoturbation results in the mixing of soil materials. As a result of cryoturbation, soil horizons are distorted, discontinuous, and broken (Höefle et al., 1998). Because of their ice-rich, disrupted and mixed nature, many cryoturbated soil horizons lack sufficient contrast in dielectric properties or are too closely spaced to be resolved with GPR. Previous GPR studies at Barrow (Hinkel et al., 2001) demonstrated that the most conspicuous subsurface reflectors observed on two-dimensional (2D) radar records, which were collected with a 400 MHz antenna, are ice wedges. Contrasts in dielectric properties between an ice wedge and the adjacent permafrost materials are generally sufficient to produce identifiable, high-amplitude reflections. Also, because of the presence of an ice-rich layer at the base of the active layer, the long-term position of the permafrost table, though weakly expressed and often partially obscured by reflections from overlying soil interfaces, is identifiable on some radar records.

Three-dimensional GPR Images:

In recent years, improved signal processing programs have enabled three-dimensional (3D) displays of two-dimensional (2D) radar records as GPR pseudo-images. Three-dimensional GPR provides greater clarity and more detailed subsurface structural information than are possible from 2D GPR (Grasmueck and Green, 1996). Three-dimensional GPR also can aid the identification of weakly expressed subsurface features and patterns. Under favorable conditions, 3D imaging of radar data can facilitate the interpretation of spatial relationships and the analysis of structural and stratigraphic features.

The acquisition of data for 3D pseudo-images requires greater expenditures of time and labor than 2D radar records. To construct a 3D pseudo-image of the subsurface, a relatively small area (typically 1-50 m²) is intensively surveyed with multiple, closely-spaced (typically at intervals of 0.1 to 1.0 m), parallel GPR traverses. A relatively dense network of closely-spaced parallel GPR traverses is necessary to resolve the geometries and sizes of different subsurface features and to prevent spatially aliasing the data (Grasmueck and Green, 1996). Data from these closely-spaced GPR traverse lines are processed into a 3D pseudo-image. Once processed, arbitrary cross-sections, insets, and time-slices can be extracted from the 3D data set. Three-dimensional imaging permits the rapid display of the data volume from different directions and cross-sections. Some software packages allow the observer to travel through the entire data volume with animated imagery (Grasmueck, 1996). Lehmann and Green (1999) provide a detailed discussion of some important considerations for carrying out 3D GPR surveys.

In recent years, a sophisticated type of data manipulation, known as *amplitude-slice-map analysis*, has been used in some GPR investigations (Conyers and Goodman, 1997). In this analysis of GPR data, a 3D pseudo-image is analyzed in "time-slices" that examine amplitude differences within specified depth intervals (Conyers and Goodman, 1997). Time-slice data are created using the spatially averaged amplitudes of radar reflections. The reflected energy is averaged horizontally between each set of parallel, 2D radar records and in a specified time window to create a time-slice. Each amplitude time-slice shows the spatial distribution of reflected wave amplitudes, which are often indicative of changes in soil properties or the presence of subsurface features.

Because of the time required to conduct fieldwork over limited areas and to process the radar data, the use of 3D pseudo-images has been restricted (Binningsbo et al., 2000). However, studies using 3D GPR have imaged the configuration of ice and sediment-filled wedge networks (Munroe et al., 2007; Doolittle and Nelson, 2008 and 2009; Godfrey et al., 2008) and estimated the 3D variation in active-layer thickness (Brosten et al., 2009).

Equipment:

The radar unit is the TerraSIRch Subsurface Interface Radar (SIR) System-3000, manufactured by Geophysical Survey Systems, Inc. (GSSI; Salem, New Hampshire).¹ The SIR System-3000 weighs about 9 lbs (4.1 kg) and is backpack portable. With an antenna, this system requires two people to operate. A 400 MHz antenna was used in this investigation.

Radar records contained in this report were processed with the RADAN for Windows (version 6.6) software program (GSSI, Salem, New Hampshire).¹ Processing included setting the initial pulse to time zero, color transformation, marker editing, distance normalization, migration, high pass horizontal filtration, and range gain adjustments. Most radar records were migrated to reduce hyperbola diffractions and to correct the geometry of subsurface interfaces. Radar records from the grid site were processed into 3D pseudo-images using the 3D QuickDraw for RADAN Windows NT software (GSSI, Salem, New Hampshire).¹ Once processed into a 3D cube, arbitrary cross sections and time-slices were viewed, and selected images attached to this report.

Study Area:

Study areas are located near Barrow, Alaska, at the northern extremity of the Arctic Coastal Plain physiographic unit (Wahrhaftig, 1965). Barrow has a cold maritime climate. The mean annual air temperature is about -12°C (Hinkel et al., 2003). Mean annual precipitation is 106 mm, with about 63% falling as rain during the months of July through September (Hinkel et al., 2003). The area is underlain by continuous permafrost. At Barrow, the thickness of permafrost is greater than 400 meters (Hinkel et al., 2003). The depth of maximum seasonal thaw (active layer) varies from about 30 to 90 cm (Hinkel and Nelson, 2003).

The Arctic Coastal Plain is characterized by multiple thaw lakes that are elongated in a north-northwesterly direction (Ping et al., 2004). Relatively thick organic layers form on the bottoms of the thaw lakes (Höefle et al., 1998). Low-centered polygons are common on younger thaw lake surfaces, while high-centered polygons dominate older thaw lake surfaces (Ping et al., 2004). Typically, soils on low-centered polygons are Typic Aquorthels, Aquic Molliturbels and Typic Histoturbels (Höefle et al., 1998; Ping et al., 2004). Soils on high-centered polygons are typically classified as Typic Historthels, Aquic Molliturbels, and Ruptic-Histic Aquiturbels (Bockheim et al., 1998; Ping et al., 2004). Soils in furrows, which overly ice-wedges, are classified as Glacis Aquorthels (Höefle et al., 1998).

Typically, in the Barrow area, the upper two meters of the soil profiles contain 50 to 75 percent segregated ice by volume (Sellmann et al., 1975). This ice occurs in pores, lenses, massive layers, and ice wedges. Finer ice lenses often occur in the upper part of the mineral soils as a result of the relatively rapid freezing of water from the surface downwards (Brown, 1967). In the lower part of mineral soils, relatively thick (5 to 10 cm) horizontal ice lenses develop as a result of the migration and freezing of soil water from the permafrost table upwards (Brown, 1967). Ice lenses, ice nets, and ataxitic ground ice fabrics are concentrated at the base of the active layer (Höefle et al., 1998).

¹ Manufacturer's names are provided for specific information; use does not constitute endorsement.

The *Grid Site* is located on an older thaw lake basin that contains multiple frost boils and high-center polygons. Long-term, thermal and soil moisture monitoring instruments are located adjacent to the *Grid Site*. At the time of the survey, the surface was covered with about 20 to 60 cm of hard packed snow, which was thinner on high-center polygons and thicker in furrows. Firm snow has a very low relative dielectric permittivity (0.1 to 2; Daniels, 2004), which results in a higher radar propagation velocity than through the silty permafrost (4 to 8; Daniels, 2004). While snow cover provided easy access to the study sites by snowmobiles and coring equipment, its variable thickness affected the accuracy of depth interpretations.

Field Methods:

A grid was established at the *Grid Site*. To expedite GPR field work, two 50-m length and parallel base lines were established across the site. The length of these two parallel lines was equal to the distance separating them. The two parallel base lines defined a 2500 square meter (0.25 ha) grid area. Along each base line, survey flags were inserted in the ground at an interval of 50 cm. For positional accuracy, GPR traverses were completed along a reference line, which was tightly stretched between similarly numbered flags on the two parallel base lines. Along the reference line, marks were spaced at 100 cm intervals. As the antenna was towed passed each reference mark, a vertical mark was impressed on the radar record to provide distance control. The GPR survey was completed by walking, in a back and forth manner with the antenna and the GPR control unit, along the reference line, which was moved sequentially across the grid area between similarly numbered flags on the two parallel base lines.

Calibration:

Ground-penetrating radar is a time scaled system. The system measures the time that it takes electromagnetic energy to travel from an antenna to an interface (e.g., soil horizon, stratigraphic layer, and ice-wedge) and back. To convert the travel time into a depth scale, either the velocity of pulse propagation or the depth to a reflector must be known. The relationships among depth (D), two-way pulse travel time (T), and velocity of propagation (v) are described in equation [1] (after Daniels, 2004):

$$v = 2D/T \quad [1]$$

The velocity of propagation is principally affected by the relative dielectric permittivity (E_r) of the profiled material(s) according to equation [2] (after Daniels, 2004):

$$E_r = (C/v)^2 \quad [2]$$

Where C represents the speed of light in a vacuum (0.3 m/ns). Typically, velocity is expressed in meters per nanosecond (ns). In soils, the amount and physical state (temperature dependent) of water have the greatest effect on the E_r and v. The relative dielectric permittivity ranges from 1 for air, to 78 to 88 for water (Cassidy, 2009). Small increments in soil moisture can therefore result in substantial increases in the relative dielectric permittivity of soils (Daniels, 2004). Singh et al. (2011) using a 1000 MHz antenna over different snow packs estimated relative dielectric permittivity to range from 1.86 to 3.69. Differences in these E_r estimates were associated with differences in snow wetness and density.

Table 1
Referenced relative dielectric permittivity (E_r) and propagation velocity (v)
for materials encountered at Barrow, Alaska.

Material	E_r	v	Source
Ice	3 to 4	0.173 to 0.150 m/ns	Conyers and Goodman, 1997
Permafrost	4 to 8	0.150 to 0.106 m/ns	Daniels et al., 2004
Snow	0.2 to 3.7	0.671 to 0.156 m/ns	Daniels et al., 2004; Singh et al. 2011

Typical values for the E_r and v for the ice, permafrost and snow are listed in Table 1. Arcone and Delaney (1982) estimated the E_r of permafrost in the ice-rich, organic silts near Barrow, Alaska, to range between 4 and 5. These

values for permafrost remain constant below temperatures of -3°C , but rise significantly as the soil temperature rises above -2°C and more free water is present in the soil (Arcone et al., 1982).

In previous GPR investigations at Barrow, based on the depths to known reflectors that were observed in seven cores, E_r averaged 5.2 and ranged from 3.4 to 7.7 in the upper 1 m of the soil profile (Hinkel et al., 2001). In this study, based on the measured depth to the top of a buried ice wedge and velocity analysis (hyperbola matching techniques), an averaged E_r of 5.43 ($v = 0.1288\text{ m/ns}$) was used. Spatial variations in snow thickness, ice contents and soil materials, however, were known to exist within the *Grid Site*. The E_r of snow varies with its moisture content and density (Singh et al., 2011), and variations in these parameters will introduce errors into depth calculations. As a consequence, depth estimates used in this report should be viewed as close approximations.

Interpretations:

2D Radar Records of Ice-Wedges

Figure 3 contains two images of the same radar record from the *Grid Site*. These images are from a portion of the radar record that was collected along line $Y = 46.5\text{ m}$. For both images, the horizontal scale represents units of distance and is expressed in meters. The short, white, vertical lines at the top of the images represent equally-spaced (1 m) reference points. The vertical scale represents the two-way pulse travel time and is expressed in nanoseconds (ns). The upper image represents a minimally processed radar record. Processing has been limited to time-zero position correction, horizontal scale normalization, color table and transform selection, and display gain. In the lower image, additional processing was used and included signal stacking (to remove high frequency noise, which appears as “snow” on the upper radar record) and high pass infinite impulse response filter (to remove low frequency noise, which appears as wider, flat-lying, horizontal bands on the upper radar record). The numbered arrows at the top of Figure 3 represent the location of core sites.

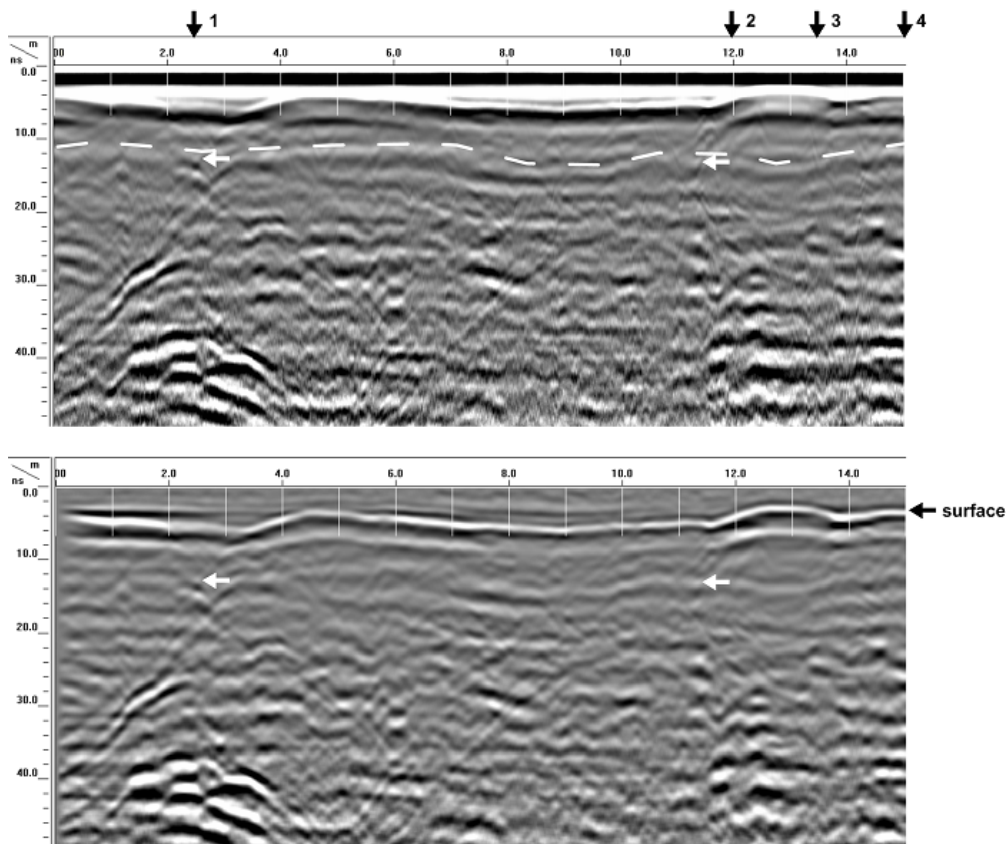


Figure 3. A portion of the 2D radar record that was collected along line $Y = 46.5\text{ m}$. Core sites are located and labeled at the top. All measurements are in meters.

On the upper radar record shown in Figure 3, because of strong reflections from the ground and air waves and the relatively thin snow cover, the snow/soil interface is difficult to discern. After processing, which removed parallel bands of low frequency noise and reflections from the air/soil interface, the wavy boundary of the snow/soil interface is more easily traced across the radar record (see lower record in Figure 3). On this radar record, the snow cover is generally less than 35 cm, but deepens to as much as 45 to 50 cm thick over two minor concavities or furrows. These slight furrows or depressions were presumed to overly and indicate the presence of ice wedges. Soil cores were extracted in each of these furrows (see “1” and “2” in Figure 3). The core extracted from site 1, revealed 50 cm of snow overlying 10 cm of organic materials and 35 cm of mixed and convoluted soil materials. An ice wedge was encountered at a soil depth of 45 cm. The reflector associated with the top of the ice wedge occurs at a time interval of about 13 ns (white-colored arrows indicates the approximate position of the ice-wedge tops). In Figure 3, a second core (“2”) was extracted at the 12 m distance mark, but failed to intercept an ice-wedge. However, after later examination of this radar record, this core was found to penetrate the edges and was not located in the center and deepest portion of the furrow.

The tops of the two ice wedges are difficult to discern on the radar records shown in Figure 3. These features are more evident on the less processed upper radar record, where more prominent diffraction tails dip away from the ice wedges. At deeper depths (time intervals) beneath and to the sides of the cored ice wedge (“1” in Figure 3), larger and more pronounced hyperbola and diffraction tails are evident. These more strongly expressed multiple hyperbolas begin at a time interval of about 36 ns. Using the estimated velocity of pulse propagation ($v = 0.1288$ m/ns), this group of hyperbolas occur at an estimated depth of about 2.35 m. As the core did not extend to this depth, the features producing these lower hyperbolas are unknown.

Arcone et al. (1982) observed that ice wedges produce hyperbolic reflection patterns when passed over by a GPR antenna. Hyperbolic reflections are produced by the antenna’s wide arc of radiation and signal diffraction. The peak of a hyperbola should correspond to the top of an ice-wedge. Several investigators (Arcone et al., 1982; Kettles and Robinson, 1997; Hinkel et al., 2001; Fortier and Allard, 2004; Munroe et al 2007; and De Pascale et al. 2008) have observed that the principal reflection hyperbola produced by the top of an ice wedge is difficult to distinguish on most radar records. This is because the top of an ice wedge often occurs at shallow soil depths where its reflections are partially obscured and distorted by reflections from near surface soil layers and features. Arcone et al. (1982) observed that, where apparent, an individual ice-wedge often consists of multiple hyperbolas and diffraction patterns. Under these conditions, the “true peak” is masked by the superposition of several hyperbolic bands and linear reflections.

Directly beneath the principal reflection hyperbola, secondary hyperbolas often occur. These hyperbolas have been associated with refractions of the propagated waveform inside the ice wedge and oblique reflections from the vertically foliated ice and the ice-wedge wall. Secondary hyperbolas that occur at a longer time interval beneath ice wedges may represent edge diffractions within the wedge structure or soil inhomogeneities. Inhomogeneities can cause constructive or destructive interference, which fosters misleading signal geometries and amplitudes (Fortier and Allard, 2004). Fortier and Allard (2004) describe these secondary, multiple hyperbolic reflections as forming a distinguishing *hyperbolic facies* that can aid the identification of ice wedges.

Bertram et al. (1972) also observed multiple, hyperbolic reflections on radar records that corresponded with the position of ice wedges in high center, ice-wedge polygons near Barrow, Alaska. Based on their interpretation, which were made after several deep excavations along the radar traverse line, these reflections are associated with the bottom of the ice wedges (at depths ranging from about 2.4 to 2.7 m) and the contact with the underlying soil materials. The depths ascribed by Bertram et al. (1972) to these secondary hyperbolas are close to the depth estimated for the secondary group of hyperbolas shown in Figure 3 (2.35 m). Fortier and Allard (2004), in a study of low center polygons on Bylot Island, also associated the deeper reflections to the bottom of the ice wedges. Kettles and Robinson (1997) observed inconsistent reflection amplitudes under small ice-wedge depressions, while larger ice wedges displayed deeper reverberations or *wave trains* similar to the ones shown on the radar record in Figure 3.

Other, more subtle features on the radar record can provide additional clues as to the presence of ice wedges. Abrupt changes in the ground-surface topography are associated with ice wedge furrows. As the radar antenna is

pulled across a trough, differences in reflected signal amplitudes can be produced by changes in ground coupling and snow-depth, and beam focusing resulting from surface roughness. Muted or interrupted reflection patterns have been used by some to infer the presence of massive ground-ice bodies (Moorman et al., 2003). De Pascale et al. (2008) associated near-vertical disruptions in planar reflection patterns with ice wedges. On the radar records shown in Figure 3, disrupted radar patterns are evident near core site “1”, the site underlain by an ice wedge. Similar radar reflection patterns suggest the presence of an ice wedge to the immediate left of core site “2”. However, this feature was not cored to verify this interpretation.

In the upper radar record shown in Figure 3, a white-colored, segmented line has been used to highlight an interface that is believed to represent the permafrost table. This interface occurs at estimated depths ranging from about 70 to 100 cm. Hinkel et al. (2001) demonstrated that the long-term position of the permafrost table can be traced laterally across some radar records because of ice-enrichment immediately below the active layer. On this radar record, this interface, though continuous, appears weakly expressed and slightly wavy.

Below the permafrost table, radar reflections become more chaotic and less planar, possibly suggesting an abundance of segregated ice. In Figure 3, the core extracted from site “2” revealed an active frost boil with *ataxitic* cryogenic fabric occurring at a depth of 82 to 111 cm (maximum depth of coring). *Ataxitic* fabric is very ice-rich with soil aggregates appearing to be suspended in the ice (Ping et al., 2004). The high ice content of this *ataxitic* fabric is presumed to be responsible for some of the higher-amplitude reflections evident in the middle and lower parts of this radar record

Three-Dimensional Pseudo-Images of Ice-Wedges:

Figure 4 contains two 3D-cube displays of the *Grid Site*. In Figure 4, the cube on the left (see A) is solid, the cube on the right (see B) is a solid cube with a 42 by 42 by 2.4 m inset cube removed. In these displays, all scales are in meters. The depth scale assumes a constant propagation velocity of about 0.13 m/ns. For display purposes, the vertical scale of these cubes has been highly exaggerated. The grid’s origin is located in the southeast corner of these 3D-cube displays. The X axis is in the right foreground, the Y axis is in the left foreground.

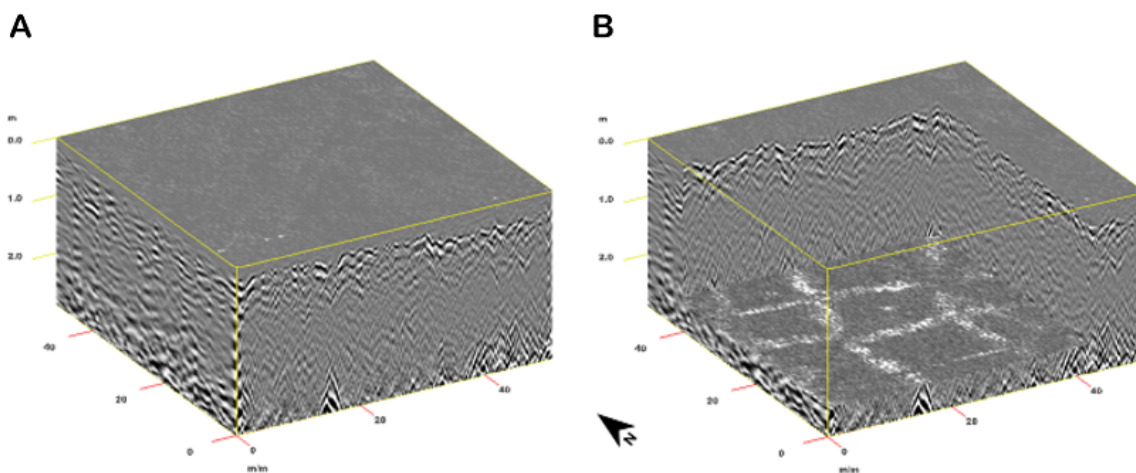


Figure 4. A solid cube and a cube with a 42 by 42 by 2.4 m inset removed.

All radar traverses were conducted parallel to the X axis, which is orientated in an east-west direction. As a consequence, sample traces overlap in this direction and the original signals are recovered in the data. In processing the 3D image, as radar data were not continuously recorded along the Y axis, but at 50-cm intervals, the data had to be reconstructed. As a consequence of this process, compared with the X axis, sample traces are more widely spaced along the Y axis. This has resulted in data omission, interpolation and aliasing along the Y axis. Consequently, along the Y axis, radar data appear noticeably *smudged*, less resolved, and more generalized.

In the solid cube display (Figure 4A); the most noticeable reflectors along the sidewalls are the snow-soil interface in the upper part and multiple high-amplitude diffractions in the lower part of the profiled materials. Reflections from the snow-soil interface appear uneven and discontinuous. However, these reflection patterns are essentially parallel with the top of the cube. Segmentation of this reflector is presumably the result of the uneven ground surface and the scattering of radar energy. The hyperbolas in the lower part of the profiled materials are due to lateral truncations in bedding planes and/or presence of dissimilar materials. Higher amplitude radar reflections are generally absent in the 1 to 2 m depth interval. In the solid cube, there is little graphic evidence, which would suggest the presence of ice wedges and polygonal pattern ground.

In the solid cube with a 42 by 42 by 2.4 m inset cube removed (Figure 4B), intersecting lines are noticeable on the base of the cutout cube. These intersecting, linear features are the result of ice wedges. The spatial patterns evident along the base of the cutout cube help define the geometry of ice wedge polygons. As evident on the exposed sidewall in the right foreground, these horizontal features form hyperbolas in vertical cross section. The reflections from the ice-wedges vary in width and appear discontinuous in some places.

Figure 5 contains six time-slice images of the subsurface within *Grid Site*. The time-slices represent horizontal depth sections through the 3D cube. These slices are useful, as they allow subsurface geometric details to be recognized. In each plot, the horizontal depth section is viewed from directly overhead with the origin located in the southwest corner of the site (lower-left hand corner).

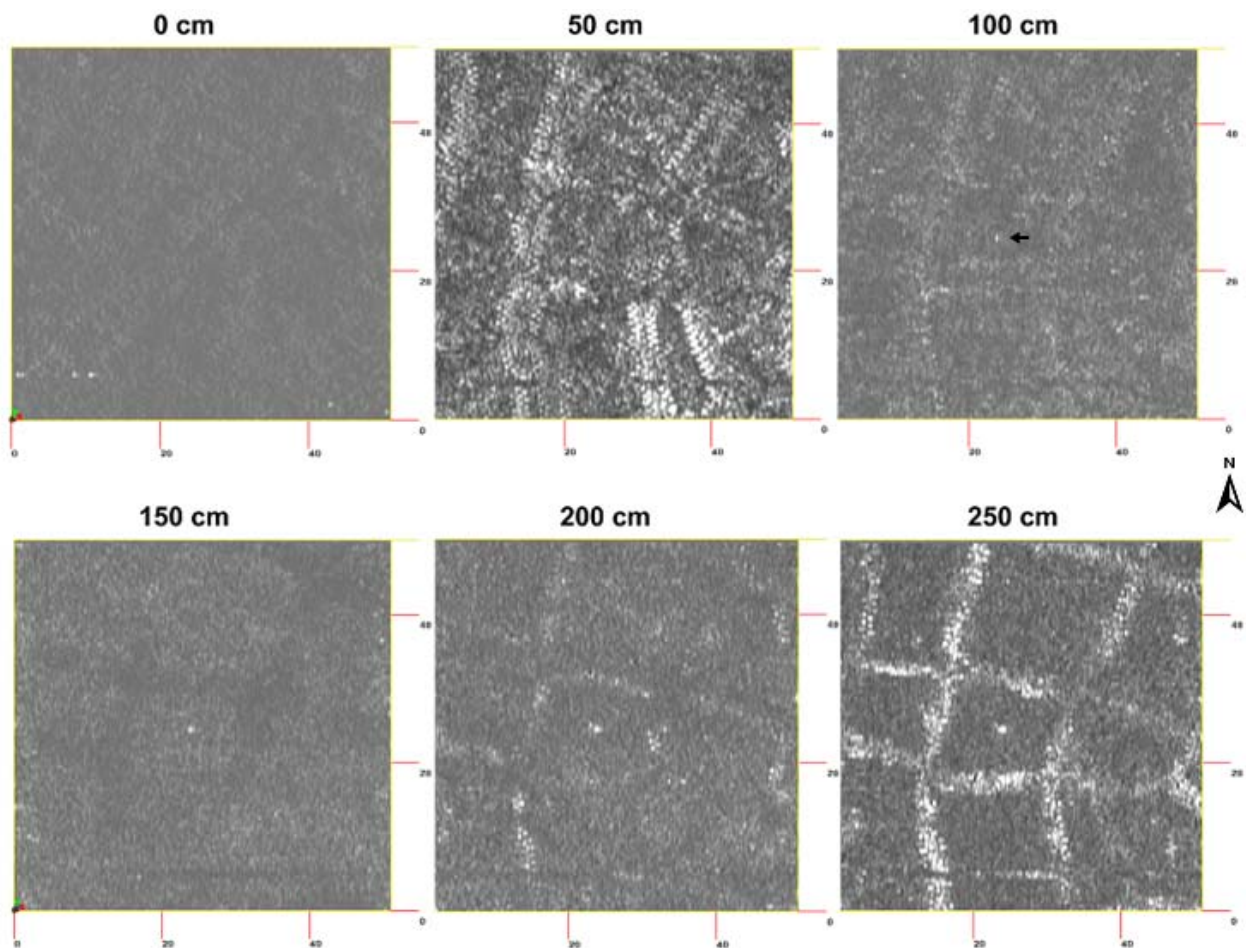


Figure 5. A series of six horizontal amplitude-slice images from the Grid Site. The approximate depth of the horizontal time-slice is indicated above each image. The geometry of furrows and ice-wedges are clearly visible in the 50- and 250-cm depth slices, respectively

In Figure 5, the 0-cm slice represents the air/snow interface, which on this processed image is nondescript and consists of low-amplitude signals. This amplitude-slice image is essentially devoid of any noteworthy reflections. On the 50-cm slice, the uneven snow-soil interface has been intermittently intercepted. On this image, high-amplitude (colored white) reflections represent the intersection of this horizontal depth-slice image with the uneven snow-soil interface. The linear patterns evident in this image mirror the approximate position of the ice-wedge furrows. These features have a distinct herringbone appearance, which is the result of reflection positioning errors on the synthesized 3D pseudo-image. A high-amplitude point reflector has been identified with an arrow on the 100-cm depth slice. With the exception of the 0-cm amplitude-slice image, this reflector is evident on all images and is assumed to represent a buried metallic artifact (e.g., probe or metal rod).

In the depth-slice images shown in Figure 5, horizontal images from intermediate depths (100- to 200-cm) are largely devoid of high-amplitude reflections. This indicates uniform or homogenous materials. However, within this depth interval, weakly expressed, linear reflections continue to suggest the presence and geometry of the ice wedges. Being vertical, ice wedges would reflect less energy back to the radar antenna and would appear as low amplitude reflections. The ice-wedge network is best expressed on the 250-cm slice. The reason for the improved expression of the ice-wedges at this depth interval is presently unclear, but based on the observations of Bertram et al. (1972), is associated with the bottoms of ice-wedges and their contact with the underlying soil materials. In the 250-cm depth slice image, high-amplitude reflections form a network of well defined, lineations that intersect at various angles.

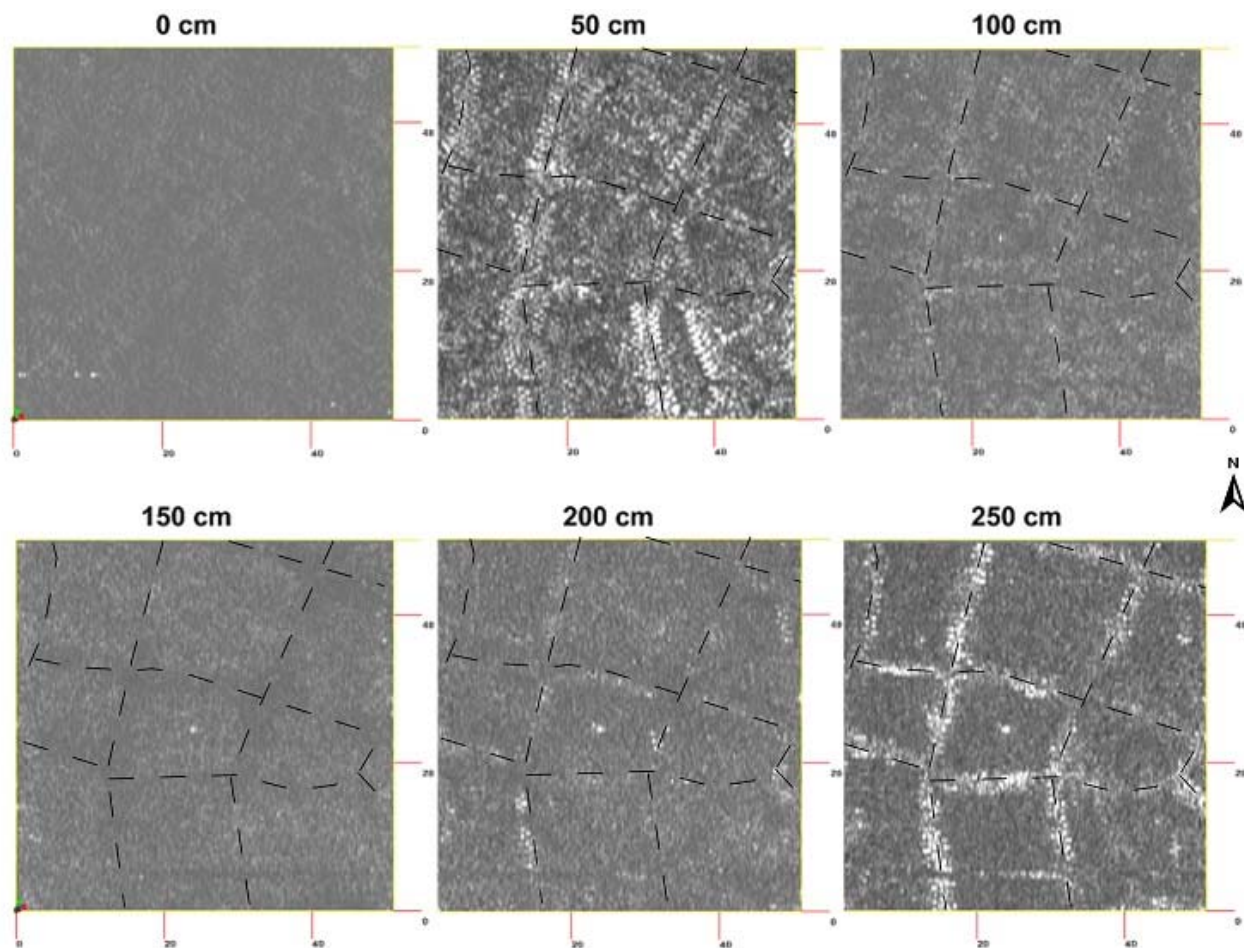


Figure 6. In this series of six, horizontal amplitude-slice images from the Grid Site, a pattern of segmented lines have been used to approximate the locations of furrows and ice wedges. The intersecting lines form a network of ice-wedge polygons.

Figure 6 contains the same six, horizontal time-slice images of *Grid Site* that were shown in Figure 5. Superimposed on most of these images is a network of segmented lines that represent the ice-wedge polygon structure. On closer review of these images, it will be noticed that the patterns indicated by the segmented lines are also expressed on all subsurface time-sliced images. The expressions of these lineations do vary in clarity and amplitude on the different depth-sliced images.

Two-Dimensional Radar Profile of a Thaw Lake:

Ground-penetrating radar has been used to resolve ice thickness, the bathymetry of ice-covered river and lake, and thermal interfaces beneath ice-covered lakes (Kovacs, 1978 and 1990; Arcone and Delaney, 1987; Best et al., 2005; Stevens et al., 2009). During this investigation episode, a GPR traverse was also conducted across the frozen surface of a thaw lake near Barrow. Figure 7 is the radar record of this traverse. In Figure 7, all scales are in meters. The depth scale assumes a constant propagation velocity of about 0.13 m/ns. On this radar record, the vertical scale has been greatly exaggerated for display purposes.

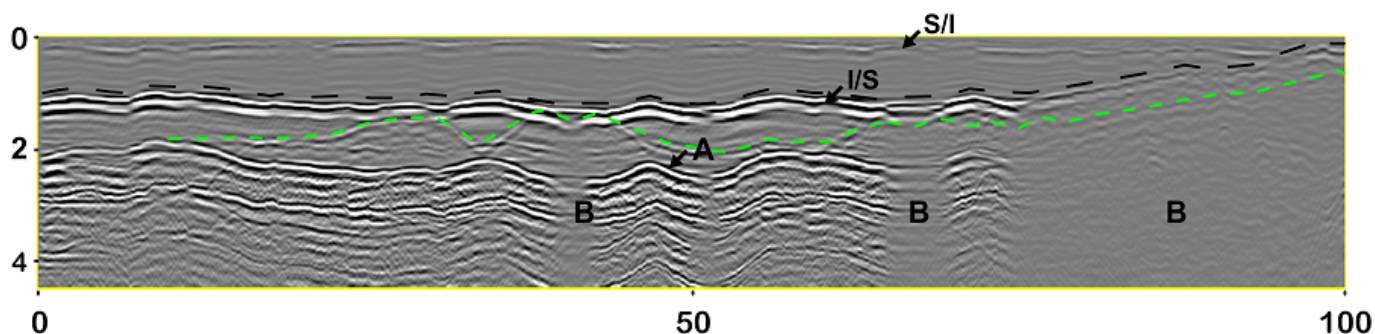


Figure 7. This radar record was collected across a margin of a thaw lake. All scales are expressed in meters.

On the radar record shown in Figure 7, the major reflectors identified are: the snow/ice interface (S/I), the ice/soil interface (I/S), and ice-bottom multiples (A). The snow/ice interface (S/I) is represented by comparatively low-amplitude, horizontal reflections that closely parallels the top of the radar record. The ice/soil (I/S) interface is the most strongly expressed subsurface interface on this radar record. A black-colored segmented line has been used to highlight this interface. In this portion of the thaw lake, the water appears to be completely frozen with no apparent reflections from pools of free water, which would be located above the reflections from ice/soil interface. In Figure 7, the depth to the ice/soil interface thins towards the right-hand portion of the radar record where the boundary of the lake is crossed. In the right-hand portion of this radar record, as the ice/soil interface becomes shallower, the amplitude of the reflected signals weakens suggesting a more transitional and less abrupt interface. Though unknown at this time, the lessening of the signal amplitudes from this interfaces can be attributed to scattering losses from segregated ice crystals and the presence of free water.

On the radar record shown in Figure 7, several sets of double reflections or ice-bottom multiples are evident. These multiples (see A) are from and mimic the ice bottom reflections. The multiples represent the double reflections of a portion of the reflected energy within the ice producing the secondary reflections shown on this radar record. Also in Figure 7, several distinct zones of signal weakening have been identified (see “B”). While the source(s) of signal attenuation is unknown due to the lack of core observations, it is attributed to scattering losses from segregated ice crystals and the presence of greater amounts of free water.

In Figure 7, a green-colored, segment line has been used to identify a weakly expressed subsurface interface. This interface appears wavy beneath the deeper portions of the thaw lake, but becomes more parallel with the ice/soil interface as the ice thins and the lake shallows. While the identity of this interface is presently unknown it is believed to represent the permafrost table.

Two-Dimensional Radar Profile across ATV trails:

Across the North Slope of Alaska, semi-permanent trails have been created by all-terrain vehicles ("four-wheelers") during warmer summer months. The most noticeable affects of these trails has been the destruction of the

vegetation cover. The destruction of the vegetal covering will increase soil temperatures, thaw and subsidence, which will result in increased soil moisture contents as water finds its way into the topographic depression created by subsidence. Ground-penetrating radar was used to obtain an image of the subsurface across one of these trails. It was hypothesized that GPR could be used to assess the depth to the permafrost table under the trail and determine whether the top of the ice-rich layer has been depressed with respect to the surrounding areas. It was assumed that the radar traverse would show a depression under the trail.

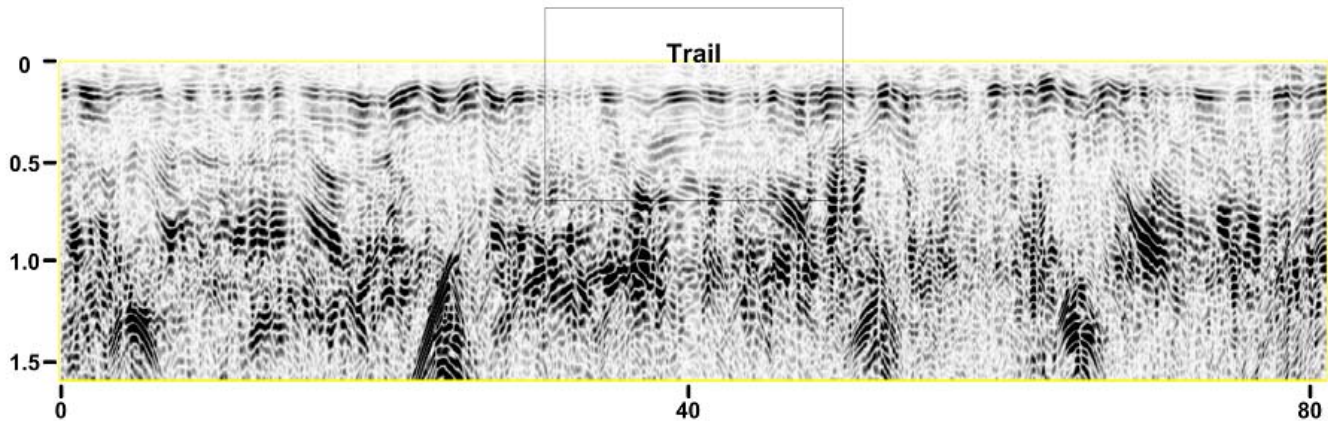


Figure 8. This portion of a radar record was collected across an Arctic trail. The approximate position of the trail has been enclosed by a rectangle.

Figure 8 is a portion of a radar record that was collected over a snowmobile trail. In Figure 8, all scales are expressed in meters. The depth scale assumes a constant propagation velocity of about 0.13 m/ns. This radar record has been vertically exaggerated for display purposes. The approximate position of the trail is included within the rectangle drawn on this radar record. Near the top of this radar record, the dark-colored, high-amplitude, horizontal, planar reflector represents the snow-soil interface. The interpreted depth to this interface ranged from about 0.1 to 81 cm and averaged 40 cm (using a propagation velocity of 0.1288 m/ns and Equation [1]).

On the radar record shown in Figure 8, the location of the trail is difficult to discern by subsurface imagery alone. When lead to the subsurface area enclosed by the rectangle, the viewer may perceive altered patterns or additional radar reflections in the near subsurface and attribute these features to the trail. However, there is too much ambiguity in this interpretation process. While the ability of GPR to detect differences in the subsurface is not doubted, additional field work is necessary to improve pattern recognition associated with trails on radar records. While in the field, the exact location of the trails seemed uncertain and was not confirmed. The time spent on this site with GPR was too limited. Interpretations can be improved with additional field time, more exact location of trails, and supporting core observations.

References:

- American Geological Institute, 1980. Glossary of Geology, Second Edition. American Geological Institute, Falls Church, Virginia.
- Annan, A.P. and J.L. Davis, 1976. Impulse radar sounding in permafrost. *Radio Science* 2:383-394.
- Annan, A.P., and J.L. Davis, 1978. High frequency electrical methods in the detection of the freeze-thaw interface. IN: Proceedings of the Third International Conference on Permafrost. Edmonton, Alberta. National Research Council of Canada, Ottawa. 495-500.

- Annan, A.P., J.L. Davis, and W.J. Scott, 1975. Impulse radar wide-angle reflection and refraction sounding in permafrost. Geological Survey of Canada Paper 75-1C: 335-341.
- Arcone, S.A., E.F. Chacho, and A.J. Delaney, 1998. Seasonal structure of taliks beneath arctic streams determined with ground-penetrating radar. 19-24 pp. *IN: Lewkowicz, A.G., and M. Allard (eds.) Proceeding of the 7th International Conference on Permafrost. Yellowknife, NWT, Canada, 23-27 June 1998.*
- Arcone, S.A., and A.J. Delaney, 1982. Dielectric properties of thawed active layers overlying permafrost using radar at VHF. *Radio Science* 17(3): 618-626.
- Arcone, S.A., and A.J. Delaney, 1984. Radar investigations above the Trans-Alaskan Pipeline near Fairbanks. U. S. Army Cold Regions Research and Engineering Laboratory, CRREL Report 84-27.
- Arcone, S.A., and A.J. Delaney, 1987. Airborne river-ice thickness profiling with helicopter-borne UHF short-pulse radar. *Journal of Glaciology* 33: 330-340.
- Arcone, S.A., and A.J. Delaney, 1989. Investigation of dielectric properties of some frozen materials using cross-borehole radiowave pulse transmission. CRREL Report 89-4. . S. Army Cold Regions Research and Engineering Laboratory, Hanover, New Hampshire.
- Arcone, S.A., P.V. Sellmann, and A.J. Delaney, 1982. Radar detection of ice wedges in Alaska. CRREL Report 82-43. U. S. Army Cold Regions Research and Engineering Laboratory, Hanover, New Hampshire.
- Bertram, C.L., K.J. Campbell, and S.S. Sandler, 1972. Locating large masses of ground ice with an impulse radar system. 241-260 pp. In: *Proceedings of the Eighth International Symposium on Remote Sensing of Environment. Ann Arbor, Michigan.*
- Best, H., J.P. McNamara, L. Liberty, 2005. Association of ice and river channel morphology determined using ground-penetrating radar in the Kuparuk River, Alaska. *Arctic and Alpine Research* 37: 157-162.
- Binningsbo, J., E.S. Eide, and J.F. Hjelmstad, 2000. 3D migration of GPR array-antenna data. 459-463 pp. *IN: (Noon, D. editor) Proceedings Eight International Conference on Ground-Penetrating Radar. May 23 to 26, 2000, Goldcoast, Queensland, Australia. The University of Queensland.*
- Bockheim, J.G., D.A. Walker, L.R. Everett, F.E. Nelson, and N.I. Shiklomanov, 1998. Soil and cryoturbation in moist nonacidic and acidic tundra in the Kuparuk River Basin, Arctic Alaska, U.S.A. *Arctic and Alpine Research* 30: 166-174.
- Brandt, O., K. Langley, J. Kohler, and S-E. Hamran, 2007. Detection of buried ice and sediment layers in permafrost using multi-frequency ground penetrating radar: A case examination on Svalbard. *Remote Sensing of Environment* 111: 212-227.
- Brosten, T.R., Bradford, J.H., McNamara, J.P., Gooseff, M.N., Zarnetske, J.P., Bowden, W.B., Johnston, M.E., 2009. Estimating 3D variation in active-layer thickness beneath arctic streams using ground-penetrating radar. *Journal of Hydrology* 373 (3-4), pp. 479-486
- Brown, J., 1967. Tundra soils formed over ice wedges, northern Alaska. *Soil Science Society of America Proceedings* 31: 686-691.
- Cassidy, N.J., 2009. Electrical and magnetic properties of rocks, soils, and fluids. In *Ground Penetrating Radar: Theory and Applications*, ed. H. M. Jol, 41-72 pp. Elsevier Science, Amsterdam, The Netherlands.
- Conyers, L.B., and D. Goodman, 1997. Ground-penetrating radar: An introduction for archaeologists. Altamir Press, Walnut Creek, California.

- Dallimore, S.R., and J.L. Davis, 1987. Ground-probing radar investigations of massive ground ice and near surface geology in continuous permafrost. 913-918 pp. *IN: Current Research, Part A. Geological Survey of Canada Paper 87-1A.*
- Daniels, D.J., 2004. *Ground Penetrating Radar; 2nd Edition.* The Institute of Electrical Engineers, London, United Kingdom.
- Davis, J.L., W. J. Scott, R.M. Morey, and A.P. Annan, 1976. Impulse radar experiment on permafrost near Tuktoyaktuk, Northwest Territories. *Canadian Journal of Earth Science* 13:1584-1590.
- De Pascale, G.P., W.H. Pollard, K.K. Williams, 2008. Geophysical mapping of ground ice using a combination of capacitive coupled resistivity and ground-penetrating radar, Northwest Territories, Canada. *Journal of Geophysical Research* 13: F02S90, doi: 10.1029/2006JF000585.
- Doolittle, J.A., M.A. Hardisky, and S. Black, 1992. A ground-penetrating radar study of Goodream Palsen, Newfoundland, Canada. *Arctic and Alpine Research* 24(2):173-178.
- Doolittle, J.A., M.A. Hardisky, and M.F. Gross, 1990. A ground-penetrating radar study of active layer thicknesses in areas of moist sedge and wet sedge tundra near Bethel, Alaska, U.S.A. *Arctic and Alpine Research* 22(2): 175-182.
- Doolittle J.A., and F. Nelson, 2009. Characterizing relict cryogenic macrostructures in mid-latitude area of USA with three-dimensional ground-penetrating radar. *Permafrost and Periglacial Processes* 20: 257-268.
- Doolittle, J.A., and F.E. Nelson. 2008. Using GPR to characterize cryogenic macrostructures in former periglacial areas of the USA. Proceedings of the 12th International Conference on Ground Penetrating Radar, June 16-19, 2008, Birmingham, UK. Disk
- Fortier, D., and M. Allard, 2004. Late Holocene syngenetic ice-wedge polygons development, Bylot Island, Canadian Arctic Archipelago. *Canadian Journal of Earth Science* 41: 997-1012.
- Godfrey, M.J., M.T. Bannister, D.C. Nobes, and R. S. Sletten, 2008. 3D Time-Lapse Imaging of Polygonal Patterned Ground in the McMurdo Dry Valleys of Antarctica. Proceedings of the 12th International Conference on Ground Penetrating Radar, June 16-19, 2008, Birmingham, UK. Disk
- Grasmueck, M., 1996. 3-D ground-penetrating radar applied to fracture imaging in gneiss. *Geophysics* 61(4): 1050-1064.
- Grasmueck, M., and A.G. Green, 1996. 3-D georadar mapping: Looking into the subsurface. *Environmental and Engineering Geoscience* Vol. II (2): 195-220.
- Hinkel, K.M., J. Doolittle, J. Bockheim, F.E. Nelson, R. Paetzold, J. Kimble, and R. Travis, 2001. Detection of subsurface permafrost features using ground-penetrating radar, Barrow, Alaska. *Permafrost and Periglacial Processes* 12: 179-190.
- Hinkel, K.M., W.R. Eisner, J.G. Bockheim, F.E. Nelson, K.M. Peterson, and X. Dai, 2003. Spatial extent, age, and carbon stock in drained thaw lake basins on the Barrow Peninsula, Alaska. *Arctic, Antarctic, and Alpine Research* 35 (3): 291-300.
- Hinkel, K.M., and F.E. Nelson, 2003. Spatial and temporal patterns of active layer depths at CALM sites in Northern Alaska, 1995-2000. *Journal of Geophysical Research-Atmospheres* 108(D2), 10.1029/2001JD000927.

- Höefle, C.M., C.L. Ping, and J.M. Kimble, 1998. Properties of permafrost soils on northern Seward Peninsula, northwest Alaska. *Soil Science Society of America Journal* 62(6): 1629-1639.
- Horvath, C.L., 1998. An evaluation of ground-penetrating radar for investigation of palsa evolution, Macmillan Pass, NWT, Canada. 473-478 pp. *IN: Lewkowicz, A.G., and M. Allard (eds.) Proceeding of the 7th International Conference on Permafrost, Yellowknife, 23 -37 June 1998. Collection Nordicana 57. Centre d'études nordiques Université Laval, Quebec.*
- Hussey, K.M., and R.W. Michelson, 1966. Tundra relief features near Point Barrow, Alaska. *Arctic* 19:162-184.
- Kettles, I.M., and S.D. Robinson, 1997. A ground-penetrating radar study of peat landforms in discontinuous permafrost zone near Fort Simpson, Northwest Territories, Canada. *IN: Trettin, C.C., M.F. Jurgensen, D.F. Grigal, M.R. Gale, and J.K. Jeglum (eds.) Northern Forested Wetlands, Ecology and Management. Lewis Publications, Boca Raton, Florida.*
- Kovacs, A., 1978. Remote detection of water under ice-covered lakes on the North Slope of Alaska. *Arctic* 31(4): 448-458.
- Kovacs, A., 1990. Investigation of the LIZ-3 Dew Station Water Supply Lake. Special Report 90-11. USA Cold Regions Research and Engineering Laboratory. Hanover, New Hampshire.
- Kovacs, A., and R.M. Morey, 1979. Remote detection of massive ice in permafrost along the Alyeska pipeline and the pump station feeder gas pipeline. 268-279 pp. *IN: Proceedings of the Specialty Conference on Pipelines in Adverse Environments. American Society of Civil Engineers. New Orleans, Louisiana, 15-17 January 1979.*
- Kovacs, A., and R.M. Morey, 1985. Impulse radar sounding of frozen ground. 28-40 pp. *IN: Brown, J., M.C. Metz, and P. Hoekstra (editors). Workshop on Permafrost Geophysics, Golden, Colorado, 23-24 October 1984. U. S. Army Cold Regions Research and Engineering Laboratory, Special Report 85-5.*
- Lehmann, F., and A.G. Green, 1999. Semiautomatic georadar data acquisition in three dimensions. *Geophysics*, 64(3): 719-731.
- Leopold, M., M.W. Williams, N. Caine, J. Völkel, and D. Dethier, 2011. Internal structure of the Green Lake 5 rock glacier, Colorado Front Range, USA. *Permafrost and Periglacial Processes* 22(2): 107-119.
- Mangold, N., F. Forget, F. Costard, J-Peulvast, 2005. High latitude pattern grounds on Mare: Evidence for recent melting of near-surface ground ice. *ICARUS* 174(2): 1219.pdf.
- Moorman, B.J., S.D. Robinson, and M.M. Burgess, 2003. Imaging periglacial conditions with ground-penetrating radar. *Permafrost and Periglacial Processes* 14: 319-329.
- Munroe, J.S., J.A. Doolittle, M.Z. Kanevskiy, K.M. Hinkel, F.E. Nelson, B.M. Jones. Y. Shur, and J.M. Kimble, 2007. Application of ground-penetrating radar imagery for three-dimensional visualization of near-surface structures in ice-rich permafrost, Barrow, Alaska. *Permafrost and Periglacial Processes* 18: 309-321.
- Pilon, J.A., A.P. Annan, J.L. Davis, and J.T. Gray, 1979. Comparison of thermal and radar active layer measurements in the Leaf Bay Area, Nouveau-Quebec. *Geographie Physique et Quaternaire* 23: 317-326.
- Pilon, J.A., A.P. Annan, and J.L. Davis, 1985. Monitoring permafrost ground conditions with ground probing radar (G.P.R.) 71-73 pp. *IN: Brown, J., M.C. Metz, and P. Hoekstra (editors). Workshop on Permafrost Geophysics, Golden, Colorado, 23-24 October 1984. U. S. Army Cold Regions Research and Engineering Laboratory, Special Report 85-5.*

- Ping, C-L., M.H. Clark, and D.K. Swanson, 2004. Chapter 2. Cryosols in Alaska. 71-94 pp. *IN: Kimble, J. (editor) Cryosols-Permafrost-Affected Soils*. Springer, Verlag Berlin Heidelberg, New York.
- Price, L.W., 1972. The Periglacial Environment, Permafrost, and Man. Commission of College Geography, Resource Paper No. 14. Association of American Geographers, Washington, DC.
- Robinson, S.D., B.J. Moorman, A.S. Judge, and S.R. Dallimore, 1993. The characterization of massive ice at Yaya Lake, Northwest Territories using radar stratigraphy techniques. 23-32 pp. *IN: Current Research, Part B. Geological Survey of Canada, Paper 93-1B*.
- Ross, N., C. Harris, H.H. Christiansen, and B.J. Brabham, 2005. Ground penetrating radar investigations of open system pingos, Adventdalen, Svalbard. *Norwegian Journal of Geography* 59: 129-138.
- Scott, W.J., P. Sellmann, and J.A. Hunter, 1990. Geophysics in the study of permafrost. 355-384 pp. *IN: Geotechnical and Environmental Geophysics, Vol. 1: Review and Tutorial. Society of Exploration Geophysicists Investigation in Geophysics, No. 5*.
- Sellmann, P.V., J. Brown, R.I. Lewellen, H. McKim, and C. Merry, 1975. The classification and geomorphic implications of thaw lakes on the arctic coastal plain, Alaska. U.S. Army CRREL Research Report
- Sequin, M.K., 1986. Geophysics of permafrost mounds. *Eos* 67, 1401.
- Singh, K.K., P. Datt, V. Sharma, A. Ganju, V.D. Mishra, A. Parashar, and R. Chauhan, 2011. Snow depth and snow layer interface estimation using ground penetrating radar. *Current Science* 100 (10): 1532-1539.
- Soil Survey Staff, 1999. Soil Taxonomy: A Basic System of Soil Classification for Making and Interpreting Soil Surveys. Second Edition, United States Department of Agriculture Natural Resources Conservation Service Agriculture Handbook Number 436.
- Stevens, C.W., B.J. Moorman, S.M. Solomon, C.H. Hugenholtz, 2009. Mapping subsurface conditions within near shore zone of an Arctic delta using ground penetrating radar. *Cold Region Science and Technology* 56(10): 20-28.
- Vonder Mühl, D., C. Hauck, and H. Gubler, 2002. Mapping of mountain permafrost using geophysical methods. *Progress in Physical Geography* 26(4): 643-660.
- Watanabe T., N. Matsuoka, H.H. Christiansen, A. Ikeda, 2008. Sounding ice and soil wedge structures with ground-penetrating radar. *In: Kane DL, Hinkel KM (eds) Proceedings of the Ninth International Conference on Permafrost*. Institute of Northern Engineering University of Alaska Fairbanks, Fairbanks, 1933-1938.
- Wahrhaftig, C., 1965. Physiographic Divisions of Alaska. USGS Professional Paper 482.
- Wong, J., J.R. Rossiter, G.R. Olhoeft, and D.W. Strangway, 1977. Permafrost: electrical properties of the active layer in situ. *Canadian Journal of Earth Science* 14(4): 582-586.
- Wu, T., L. Shuxun, G. Cheng, and N. Zhuotong, 2005. Using ground-penetrating radar to detect permafrost degradation in the northern limit of permafrost on the Tibetan Plateau. *Cold Regions Science and Technology* 41:211-219.
- Yoshikawa, K., C. Leuschen, A. Ikeda, K. Harada, P. Gogineni, P. Hoekstra, L. Hinzman, and N. Matsuoka, 2006. Comparison of geophysical investigations for detection of massive ground ice (pingo ice). *Journal of Geophysical Research E: Planets* 11 1 (6), art. no. E06S19.